Global insights into the fine tuning of human A2AAR conformational dynamics in a ternary complex with an engineered G protein viewed by NMR

Guillaume Ferré, Kara Anazia, Larissa O Silva, Naveen Thakur, Arka P Ray, Matthew T Eddy

Cell Reports

Global insights into the fine tuning of human $A_{2A}AR$ conformational dynamics in a ternary complex with an engineered G protein viewed by NMR

Graphical abstract

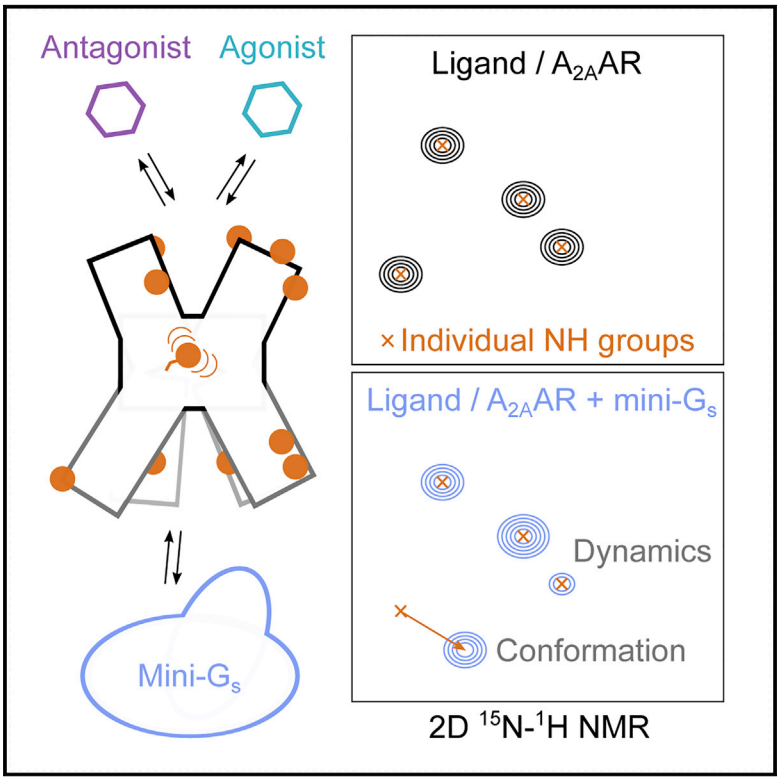

Highlights

- NMR comparison of $A_{2A}AR$ complex with agonist and ternary complex with partner protein
- Conformation of complex with agonist alone resembles active ternary complex structure
- "Fine-tuning" of receptor conformation observed for ternary complex
- Structural plasticity in key "hot spot" suggests dynamic receptor core in ternary complex

Authors

Guillaume Ferré, Kara Anazia, Larissa O. Silva, Naveen Thakur, Arka P. Ray, Matthew T. Eddy

Correspondence

matthew.eddy@chem.ufl.edu

In brief

Ferré et al. use NMR spectroscopy to reveal similar conformations of the A_{2A} adenosine receptor in complex with an agonist and a ternary complex with an engineered G protein. Observations of the toggle-switch tryptophan reveal surprising structural plasticity in the receptor core of the active ternary complex.

Ferré et al., 2022, Cell Reports *41*, 111844
December 20, 2022
https://doi.org/10.1016/j.celrep.2022.111844

Cell Reports

CellPress
OPEN ACCESS

Report

Global insights into the fine tuning of human A_{2A}AR conformational dynamics in a ternary complex with an engineered G protein viewed by NMR

Guillaume Ferré,[1,2] Kara Anazia,[1] Larissa O. Silva,[1] Naveen Thakur,[1] Arka P. Ray,[1] and Matthew T. Eddy[1,3,*]
[1]Department of Chemistry, University of Florida, Gainesville, FL 32611, USA
[2]Present address: Institut de Pharmacologie et Biologie Structurale; Université de Toulouse, CNRS, Université Paul Sabatier; Toulouse 31000, France
[3]Lead contact
*Correspondence: matthew.eddy@chem.ufl.edu
https://doi.org/10.1016/j.celrep.2022.111844

SUMMARY

G protein-coupled receptor (GPCR) conformational plasticity enables formation of ternary signaling complexes with intracellular proteins in response to binding extracellular ligands. We investigate the dynamic process of GPCR complex formation in solution with the human A_{2A} adenosine receptor (A_{2A}AR) and an engineered G_s protein, mini-G_s. 2D nuclear magnetic resonance (NMR) data with uniform stable isotope-labeled A_{2A}AR enabled a global comparison of A_{2A}AR conformations between complexes with an agonist and mini-G_s and with an agonist alone. The two conformations are similar and show subtle differences at the receptor intracellular surface, supporting a model whereby agonist binding alone is sufficient to populate a conformation resembling the active state. However, an A_{2A}AR "hot spot" connecting the extracellular ligand-binding pocket to the intracellular surface is observed to be highly dynamic in the ternary complex, suggesting a mechanism for allosteric connection between the bound G protein and the drug-binding pocket involving structural plasticity of the "toggle switch" tryptophan.

INTRODUCTION

G protein-coupled receptors (GPCRs) are key regulators of human physiology and are targeted by over 30% of FDA-approved drugs.[1] GPCR signaling proceeds through complex formation with partner proteins, including hetero-trimeric G proteins, which in turn modulate production of secondary messenger molecules.[2,3] Deciphering the molecular mechanisms underlying GPCR activation and their interactions with G proteins is thus important to better understand cellular communication and facilitate development of new therapeutics.[4,5]

Spectroscopic studies of GPCRs and their complexes complement cryoelectron microscopy (cryo-EM) and crystallographic structures by providing information on structural plasticity underlying signal transduction.[2,6] Numerous nuclear magnetic resonance (NMR) spectroscopic studies have shown that GPCRs exist in a dynamic equilibrium of multiple conformational states with relative populations related to the efficacy of bound ligands.[6–12] NMR and electron paramagnetic resonance (EPR) studies using site-specific labeling approaches also highlighted GPCR complex formation with G proteins or G protein mimetics affects additional changes in the receptor conformational equilibrium. Ternary complex formation of thermostabilized β_1-adrenergic receptor (β_1AR) with a G protein-mimicking nanobody generated a conformational state unique from the agonist-bound receptor.[13] Analogous observations were made by NMR and EPR with the β_2-AR[8,14,15] and the μ-opioid receptor (MOR).[16] Observations from these studies were interpreted to indicate weak "coupling" between the receptor orthosteric ligand-binding pocket and intracellular surface. Allosteric communication between bound G protein mimetics and the orthosteric ligand-binding pocket was also observed for thermostabilized β_1AR using ^{15}N-valine amide backbone NMR probes distributed throughout the receptor.[17–19]

Understanding the extent to which these observations can be extended to additional human GPCRs is critical to developing more universal models of cell signaling, motivating us to study this problem with the human A_{2A} adenosine receptor (A_{2A}AR). A_{2A}AR is a class A GPCR that signals through G_{olf},[20] an important protein in the brain, and G_s and regulates the cardiovascular, immune, and central nervous systems.[21–24] Deciphering the activation of A_{2A}AR has motivated the determination of 3D structures with ligands and protein partners[25–30] and NMR studies of its conformational dynamics,[31–37] making this receptor a model for studying GPCR structural biology. We leveraged a stable-isotope labeling strategy that enabled a global view of A_{2A}AR structure and dynamics upon complex formation with an engineered G_s protein. This approach allowed us to map the impact of ternary complex formation on receptor dynamics at the protein-protein interface and at a receptor "hot spot" involving the "toggle switch" tryptophan that connects the drug-binding pocket to the intracellular surface.

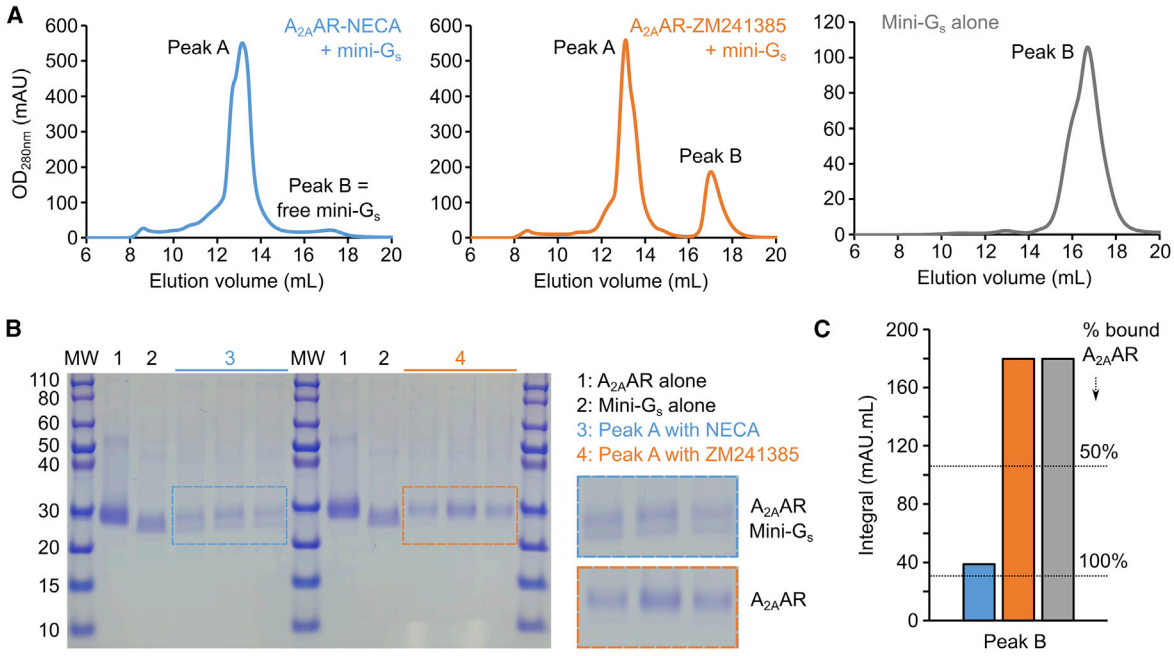

Figure 1. Validation of A_{2A}AR-mini-G_s complex formation for NMR studies

(A) Size-exclusion chromatograms of purified A_{2A}AR bound to the agonist NECA and in the presence of mini-G_s (blue), bound to the antagonist ZM241385, in the presence of mini-G_s (orange), and mini-G_s alone (gray).

(B) Annotated SDS-PAGE analysis of fractions isolated from "peak A" in chromatograms presented in (A) and isolated samples of A_{2A}AR and mini-G_s.

(C) Integrals of the free mini-G_s peak, labeled "peak B," in the SEC chromatograms presented in (A). Dotted lines indicate calculated percentages of mini-G_s-bound A_{2A}AR using a stoichiometric ratio of 1:1.2 A_{2A}AR to mini-G_s.

Our results are compared with observations from studies of other class A receptors, enabling an expanded view of GPCR signaling mechanisms.

RESULTS

Formation of agonist-stimulated A_{2A}AR ternary complexes with mini-G_s for NMR studies

To study the conformational dynamics of A_{2A}AR in complex with mini-G_s, we leveraged A_{2A}AR expression in *P. pastoris* and purification in lauryl maltose neopentyl glycol / cholesteryl hemisuccinate (LMNG/CHS) mixed micelles, demonstrated to yield folded and functional receptors.[36] The approach enabled production of A_{2A}AR samples with ^{15}N and ^{2}H stable isotopes uniformly distributed throughout the receptor. Analytical size-exclusion chromatography and SDS-PAGE showed that A_{2A}AR samples were highly pure and monomeric (Figures 1A, 1B, and S1A). To form ternary complexes, we employed the mini-G_s protein, an engineered variant of the G_s protein α-subunit.[30] Mini-G_s recapitulates G_s binding with GPCRs, including A_{2A}AR,[30,38] and its lower molecular weight is favorable for recording high-resolution NMR spectra of the ternary complex in solution. Following earlier reports,[30,38] we expressed and purified monomeric mini-G_s (Figures 1A and 1B).

We monitored A_{2A}AR ternary complex formation with the agonist NECA and mini-G_s in LMNG/CHS micelles using analytical size-exclusion chromatography (SEC) and SDS-PAGE electrophoresis (see STAR Methods; Figures 1A and 1B). Complexes were prepared with an excess of mini-G_s to obtain homogeneous preparations of A_{2A}AR bound to mini-G_s. Because A_{2A}AR binary and ternary complexes exhibited similar elution times in analytical SEC profiles, we monitored complex formation by integrating the peak of free mini-G_s (Figure 1C). Using this approach, we calculated that ~95% of the NECA-bound receptor formed monodispersed complexes with mini-G_s, in line with the SDS-PAGE analysis (Figure 1B). As expected, A_{2A}AR prepared with the antagonist ZM241385 as a control sample did not exhibit complex formation with mini-G_s (Figure 1B).

Agonist stimulation alone populates an A_{2A}AR conformation resembling the ternary complex with mini-G_s

We recorded 2D [^{15}N,^{1}H]-transverse relaxation-optimized spectroscopy (TROSY)[39] correlation spectra of [u-^{15}N,~70% ^{2}H]-A_{2A}AR in complex with the full agonist NECA and the ternary complex with NECA and mini-G_s (Figure 2). With uniform ^{15}N stable-isotope labeling, ^{15}N–^{1}H amides and ^{15}N–^{1}H tryptophan indoles provide NMR probes of local A_{2A}AR structure and conformational dynamics distributed globally throughout A_{2A}AR. The chemical shifts, line shapes, and relative intensities of these signals thus provide fingerprints of the global receptor conformation and structural plasticity related to the corresponding functional state.

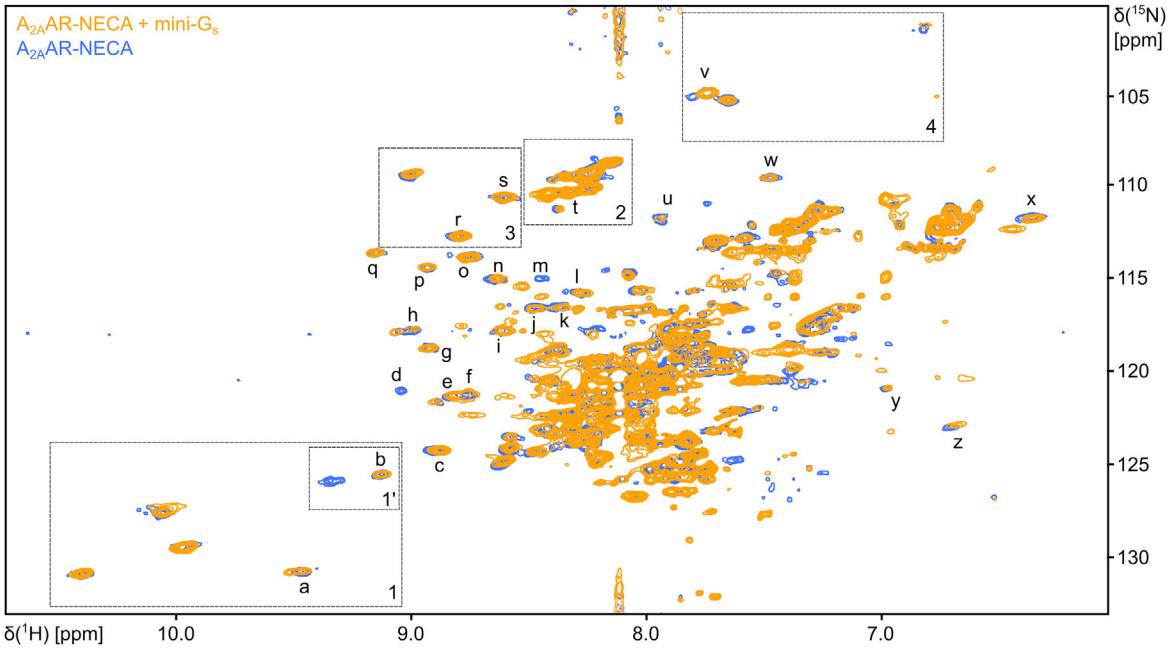

Figure 2. Comparison of structural fingerprints of $A_{2A}AR$ binary and ternary complexes

Superposition of [^{15}N,^{1}H]-TROSY correlation spectra of [u-^{15}N,~70% ^{2}H]-$A_{2A}AR$ in complex with the full agonist NECA (blue) and the ternary complex of $A_{2A}AR$ with NECA and mini-G_s (orange). Regions framed by the dotted boxes are expanded in Figure 3. Well-resolved signals indicated by the labels "a" to "z" have been used to compare structural fingerprints of $A_{2A}AR$ upon complex formation with mini-G_s.

2D [^{15}N,^{1}H]-TROSY spectra of [u-^{15}N,~70% ^{2}H]-$A_{2A}AR$ in the ternary complex with NECA and mini-G_s were well dispersed, confirming that $A_{2A}AR$ was properly folded in the ternary complex (Figure 2). The 2D TROSY spectrum of $A_{2A}AR$ in the ternary complex was distinctly different from the TROSY spectrum of $A_{2A}AR$ in complex with the antagonist ZM241385 (Figure S2). In contrast, spectra of the $A_{2A}AR$ ternary complex and the complex with the agonist NECA were highly similar, showing a significant overlap of the majority of signals (Figure 2). For signals labeled "a" to "z," selected from spectra regions greater than 8.5 or below 7.5 ppm in the ^{1}H dimension arising from backbone amide $^{15}N-^{1}H$ signals from regular secondary structure, the chemical shifts were all nearly identical. Minor changes in the TROSY spectrum of the $A_{2A}AR$ ternary complex with mini-G_s suggest subtle changes occur upon complex formation. In particular, changes in signal intensities were observed among several signals "a" to "z," suggesting differences in $A_{2A}AR$ structural plasticity between the ternary complex and the complex with agonist alone.

Functionality of $A_{2A}AR$ in the ternary complex was further confirmed by NMR-detected ligand competition experiments. With the same sample used to record the NMR data in Figure 2, NECA was displaced by adding an excess of the high-affinity antagonist ZM241385 via buffer exchange (see STAR Methods), and additional TROSY spectra were then recorded. The resulting spectrum of the ligand-exchanged sample was nearly identical to a spectrum of [u-^{15}N,~70% ^{2}H]-$A_{2A}AR$ prepared by co-purification with the ZM241385 (Figure S2B). This indicates the $A_{2A}AR$ ternary complex could be dissociated upon binding a high-affinity antagonist, resulting in a transition from the fully active to inactive $A_{2A}AR$ conformation.

Ternary complex formation tunes $A_{2A}AR$ structural plasticity at the protein-protein interface and within the transmembrane core

Because the TROSY spectra of the $A_{2A}AR$ ternary complex with NECA and mini-G_s were similar, we could reliably transfer determined assignments[36] for the tryptophan indole $^{15}N-^{1}H$ and glycine amide $^{15}N-^{1}H$ signals. These assigned $A_{2A}AR$ signals provided NMR probes throughout the receptor, including at the $A_{2A}AR$ intracellular surface, the orthosteric ligand-binding pocket, and an activation "hot spot" involving $W246^{6.48}$, the "toggle switch" tryptophan,[40,41] which connects the two regions (Figure 3A). This allowed us to quantitatively compare chemical shifts and signal intensities between the TROSY spectra of the $A_{2A}AR$ complex with NECA and the ternary complex with NECA and mini-G_s. Differences observed upon formation of the ternary complex could thus be compared with differences in chemical shifts and intensities upon binding orthosteric ligands of different efficacies (Figures 4A and 4B).

At the $A_{2A}AR$ intracellular surface, the $^{15}N-^{1}H$ indole signal of $W29^{1.55}$ (superscripts denote the Ballesteros-Weinstein nomenclature[42]), located toward the end of helix I, showed a significant chemical shift change upon ternary complex formation (Figures 3B, 4A, and 4B). We also observed a significant increase in signal intensity for $W29^{1.55}$. Previously, the line shape of the $W29^{1.55}$ $^{15}N-^{1}H$ indole signal was shown to be highly sensitive to different efficacies of bound drugs and manifested with

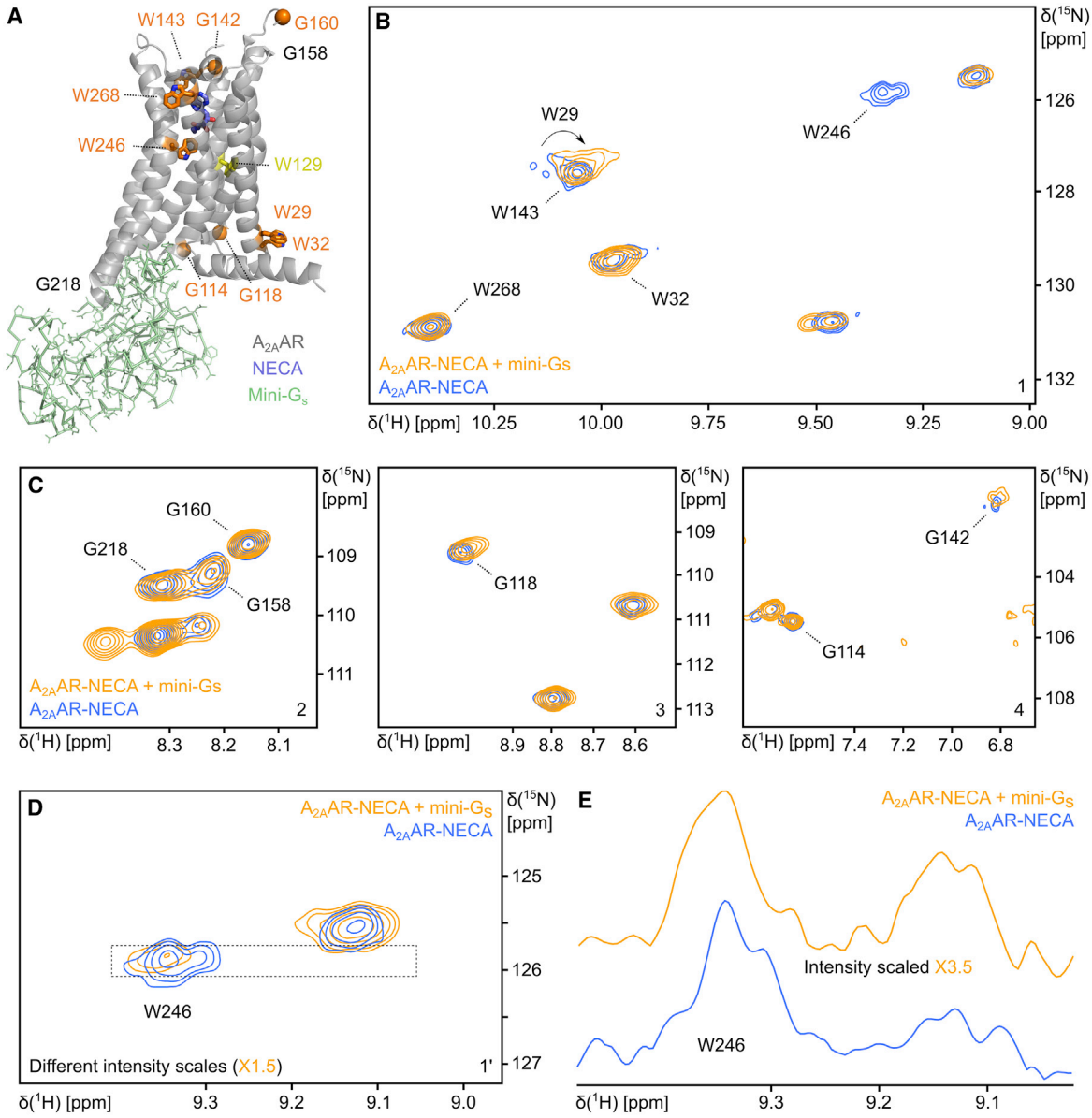

Figure 3. Site-specific views into $A_{2A}AR$ conformational changes upon ternary complex formation

(A) Assigned $A_{2A}AR$ NMR signals mapped onto the crystallographic structure of the $A_{2A}AR$ ternary complex with NECA and mini-G_s (PDB: 5G53). $A_{2A}AR$ and mini-G_s are shown in ribbon and stick representations, respectively. Assigned glycines are shown as orange spheres, and assigned tryptophans are shown in orange stick representations. G218 and G158 are labeled but not shown, as electron density were not observed in the crystal structure for these residues. W129, observed only in ZM241385-bound $A_{2A}AR$ spectra, is shown in yellow.

(B–D) Expanded views from Figure 2 with selected signals annotated. The arrow indicates an observed chemical shift change for W29.

(E) 1D projections through the ^{15}N dimension of the spectral region indicated by the dashed rectangle in (D). In (D) and (E), different intensity scales are used to display the indole $^{15}N-^{1}H$ signal for W246 in the spectrum of the ternary complex with mini-G_s, as indicated.

multiple components.[36] A rationale for this observation was the presence of structural polymorphism due to reorientation of nearby amino acids in helices VII and VIII that undergo conformational changes.[36] The chemical shift of the $W29^{1.55}$ $^{15}N-^{1}H$ indole signal for the ternary complex was different than the chemical shifts of any components for the complex with an agonist alone. Additionally, the $W32^{1.58}$ $^{15}N-^{1}H$ indole signal was significantly more intense in the $A_{2A}AR$ ternary complex (Figures 3B and 4B). Because residues in helix I do not appear to interact directly with mini-G_s in the crystal structure, the change in chemical shift $W29^{1.55}$ and intensities for $W29^{1.55}$ and $W32^{1.58}$ likely result from interactions with neighboring residues in helices VII and VIII. These data point to subtle changes in structure and potential changes in $A_{2A}AR$ conformational

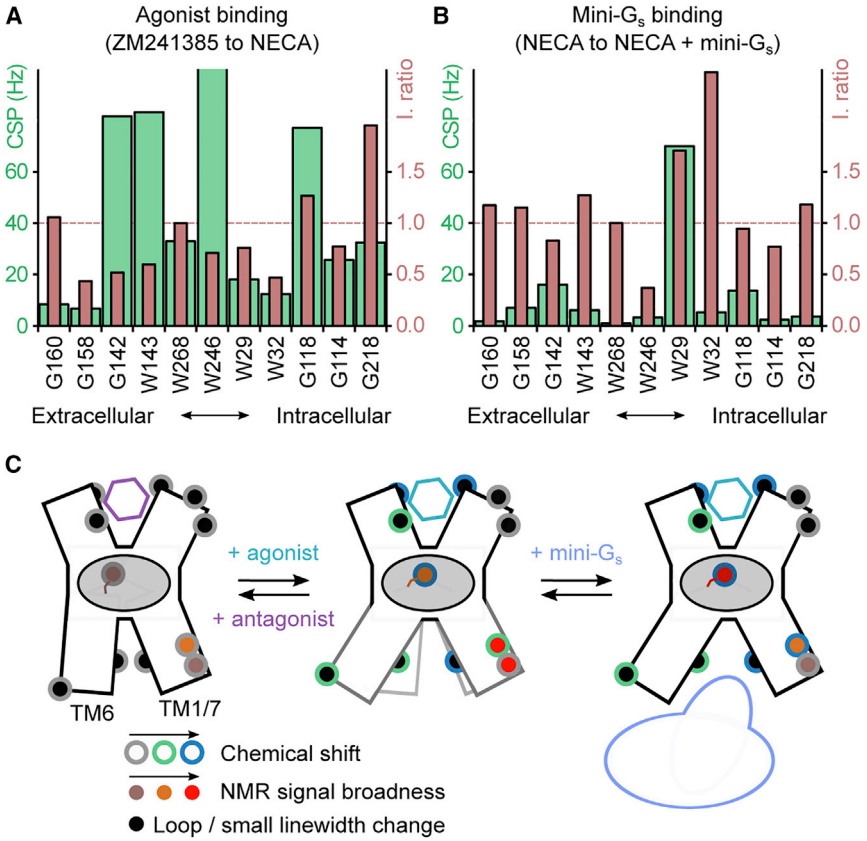

Figure 4. NMR-observed conformational changes upon agonist and mini-G_s binding

(A) Histogram comparison of chemical shift perturbations (CSPs; green) and relative intensities (I. ratio; salmon) of NMR signals of A_{2A}AR in complex with the agonist NECA with respect to signals of A_{2A}AR in complex with the antagonist ZM241385. An I. ratio >1 indicates a larger intensity observed for a signal in the spectrum of the A_{2A}AR complex with NECA relative to the spectrum for the complex with ZM241385. Chemical shift perturbations are given in units of Hertz.

(B) Histogram of CSP and I. ratio values of A_{2A}AR in the ternary complex with NECA and mini-G_s with respect to A_{2A}AR in complex with NECA.

(C) Schematic illustrating the impact of ligands and mini-G_s complex formation on the equilibrium of A_{2A}AR conformations and corresponding functional states. Assigned NMR signals are displayed as filled-in circles, with the outer layer colored to show chemical shift changes and the interior colored to indicate line broadening. The gray oval represents the particular "hot spot" region highlighted in this study, with W246$^{6.48}$ represented as a circle with lines representing different orientations of the W246 side chain in different complexes.

dynamics upon ternary complex formation. We also compared $^{15}N-^{1}H$ amide signals for G114, G118$^{4.39}$, and G218, located in intracellular loop (ICL) 2 and the intracellular ends of helices IV and VI, respectively. For all three signals, at most, only subtle differences could be observed for both chemical shifts and intensities between the A_{2A}AR ternary complex with NECA and mini-G_s and the complex with NECA (Figures 3C and 4B). This observation appears consistent with the crystal structure of the A_{2A}AR ternary complex, which shows that these residues are not in close proximity to mini-G_s and do not undergo conformational changes upon ternary complex formation. This suggests that conformations of A_{2A}AR and mini-G_s in the ternary complex are likely similar in crystals and in aqueous solution.

$^{15}N-^{1}H$ amide signals for G160 and G158, located in ECL2, and for G142$^{4.63}$, located in the extracellular end of helix IV, showed only minor changes between spectra of the A_{2A}AR ternary complex with NECA and mini-G_s and the complex with NECA (Figures 3C and 4B). Likewise, the $^{15}N-^{1}H$ indole signals for W143, located at the extracellular end of helix IV, and W268$^{7.33}$, located at the extracellular end of helix VII, were also highly similar. This indicated that the formation of the ternary complex with mini-G_s did not allosterically alter the conformation and structural plasticity of the A_{2A}AR extracellular region.

The most pronounced changes between the spectra were observed for the $^{15}N-^{1}H$ indole signal of W246$^{6.48}$, which is located in an activation "hot spot" region connecting the orthosteric ligand-binding site and receptor intracellular surface. In earlier A_{2A}AR studies, the chemical shift of W246$^{6.48}$ was shown to closely correlate with the efficacy of bound drugs, which was rationalized by ring current effects due to nearby F242$^{6.44}$.[36] F242$^{6.44}$ is a key residue of the highly conserved P$^{5.50}$–I$^{3.40}$–F$^{6.44}$ activation motif, the conformation of which strongly correlates with GPCR functional states and global conformations (Figure S4).[43] For A_{2A}AR complexes with partial agonists, W246$^{6.48}$ was observed in two different conformations, the relative populations of which depended on the efficacy of the partial agonist,[35] linking changes in partial agonist efficacy to the presence of multiple simultaneously populated receptor conformers. In the spectrum of the [u-^{15}N,~70% ^{2}H]-A_{2A}AR ternary complex, a single signal was observed for the W246$^{6.48}$ indole at the same chemical shift as observed for NECA-bound A_{2A}AR, however with a strikingly different intensity (Figures 3B, 3D, 3E, 4A, and 4B).

To confirm that the W246$^{6.48}$ $^{15}N-^{1}H$ indole signal was not significantly shifted to a different region of the TROSY spectrum, we prepared a sample of the A_{2A}AR variant W246F and recorded a TROSY spectrum of [u-^{15}N,~70% ^{2}H]-A_{2A}AR[W246F] in a ternary complex with NECA and mini-G_s. A_{2A}AR[W246F] was previously employed for signal assignment purposes and was demonstrated to be folded and functional.[36] A_{2A}AR[W246F] was monodispersed (Figure S1A), and complex formation was validated by analytical SEC and SDS-PAGE (Figures S1B and S1C). Comparing TROSY spectra of [u-^{15}N,~70% ^{2}H]-A_{2A}AR and [u-^{15}N,~70% ^{2}H]-A_{2A}AR[W246F] in ternary complexes revealed no additional signals for W246F$^{6.48}$ (Figure S3). This indicates that changes observed in Figures 2 and 3 for W246$^{6.48}$ upon ternary complex formation are due to conformational exchange broadening. Because of the strong dependence of the W246$^{6.48}$

chemical shift on nearby F242$^{6.44}$, this suggests fluctuations in the relative orientations of these two conserved residues in the allosteric coupling network within the ternary complex.

DISCUSSION

The NMR data in Figures 2 and 3 support a model of A_{2A}AR activation involving larger conformational changes upon complex formation with agonists and relatively smaller subsequent structural changes upon complex formation with mini-G_s (Figure 4C). Chemical shift and intensity changes reveal that A_{2A}AR ternary complex formation does not significantly alter the global conformation of A_{2A}AR compared with the binary complex with NECA alone. However, these data suggest that additional "fine-tuning" of the A_{2A}AR structure and conformational dynamics occur upon ternary complex formation. These observations appear to differ from NMR studies of the β_1AR,[13] β_2AR,[8,14] and MOR,[16] which reported that these receptors showed unique conformations in ternary complexes with G protein-mimicking nanobodies. This suggests that differences in signal transduction mechanisms may exist among different GPCRs despite sharing similar structural architectures and conserved residues required for activation. Our observations appear to be more in line with earlier ^{19}F-NMR studies of A_{2A}AR. ^{19}F-NMR studies of A_{2A}AR[A289C], labeled at the intracellular end of helix VII, observed large differences in the signal envelope and corresponding ensemble of conformational states between A_{2A}AR complexes with agonists and antagonists.[44] In a ^{19}F-NMR study of A_{2A}AR[V229C] in lipid nanodiscs labeled at the intracellular end of helix VI, qualitatively larger differences were observed between A_{2A}AR binary complexes with the antagonist ZM241385 and the agonist NECA than between the A_{2A}AR complex with NECA and the ternary complex with NECA and mini-G_s.[32]

For NMR probes at the receptor intracellular surface, we observed a chemical shift change for the W29$^{1.55}$ ^{15}N−^{1}H indole signal and changes in signal intensities for W29$^{1.55}$ and W32$^{1.58}$ but not for G114, G118$^{4.39}$, and G218 (Figures 3 and 4). This appears to support a view that the ternary complex structure with mini-G_s in solution was similar to that in crystals.[30] The increases in signal intensities for W29$^{1.55}$ and W32$^{1.58}$ likely result from attenuation of conformational plasticity at the receptor-mini-G_s interface. In a cryo-EM structure of A_{2A}AR in complex with the trimeric protein G_s, poorer density and higher B factors were observed in TM1,[45] suggesting that additional subtle differences may be observed between ternary complexes with mini-G_s and with trimeric G_s, as has also been proposed from ^{19}F-NMR studies.[32]

Allosteric connections between bound G proteins and GPCR orthosteric binding pockets have been observed in simulations[46] and by NMR experiments. This was manifested in studies of thermostabilized β_1AR as chemical shift changes for ^{15}N-valines located in the orthosteric binding pocket upon complex formation with a G protein-mimicking nanobody.[17,18] Upon A_{2A}AR complex formation with mini-G_s, we observed, at most, only subtle changes for residues located in the extracellular region, including those adjacent to the orthosteric ligand-binding site (Figures 2, 3, and 4). This observation suggests relatively minor modulation of the A_{2A}AR orthosteric binding pocket and extracellular region by ternary complex formation with mini-G_s.

Comparing the A_{2A}AR binary and ternary complexes, NMR data in Figures 2, 3, and 4 show significant changes observed for the W246$^{6.48}$ ^{15}N−^{1}H indole signal intensity but not chemical shift differences. The significant attenuation of the signal for W246$^{6.48}$, and the lack of a new apparent signal with a different chemical shift (Figure S3), implies that ternary complex formation with mini-G_s induced intermediate exchange of W246$^{6.48}$. The strong dependence of the W246$^{6.48}$ signal on nearby F242$^{6.44}$ indicates that the observed exchange broadening is due to dynamic reorientation of W246$^{6.48}$ with respect to F242$^{6.44}$ of the conserved P$^{5.50}$–I$^{3.40}$–F$^{6.44}$ activation motif. These data complement crystallographic and cryo-EM structures that did not show significant structural rearrangement of W246$^{6.48}$ with respect to the P$^{5.50}$-I$^{3.40}$-F$^{6.44}$ motif upon ternary complex formation. Within this context, our data suggest that understanding not just the low energy conformation of W246$^{6.48}$ observed in crystal and cryo-EM structures but also its dynamic motion is important to understanding mechanisms of A_{2A}AR signaling. W246$^{6.48}$ and nearby bulky residues have been proposed to form an "aromatic lock" whereby a break in this lock caused by agonist binding precedes larger structural rearrangements required for signaling complex formation.[47] Related to this hypothesis, computational studies indicated that W246$^{6.48}$ and nearby bulky amino acids form a hydrophobic barrier limiting water diffusion through the receptor core.[48,49] Motion of W246$^{6.48}$ was proposed to facilitate diffusion of water through the receptor and initiate subsequent larger conformational rearrangements.[48] Intriguingly, amino acid substitution of W246$^{6.48}$ or F242$^{6.44}$ appears to significantly decrease A_{2A}AR G protein signaling,[50] and for other receptors, this substitution completely abolishes G protein signaling,[51] suggesting that these residues are required to maintain structural integrity of the receptor.

In both seminal and more recent NMR studies, ring-flipping motions of aromatic residues in the cores of globular proteins have been shown to require large-scale structural rearrangements of surrounding amino acids, i.e., "breathing motions" of the surrounding protein structure.[52–54] These motions have been uniquely observed by NMR spectroscopy and hidden from crystallographic and cryo-EM structures and have been linked to consequent changes in protein function.[52–55] It is thus interesting to speculate if our observations with exchange broadening of W246$^{6.48}$ are also related to breathing motions in the core of A_{2A}AR and potentially other GPCRs and what roles these motions have in GPCR allosteric coupling between ligand-binding sites and the G protein interface.

Limitations of the study

This work presents comparative NMR studies of A_{2A}AR complexes with small molecules and a ternary complex with an agonist and mini-G_s protein. One limitation of the current work is that experiments were carried out in detergent mixed micelles containing LMNG and CHS. Although we have validated the pharmacological function of A_{2A}AR in LMNG/CHS in previous studies[36] and validated A_{2A}AR-mini-G_s complex formation in the same detergent system in the current study, this membrane mimetic does not fully capture the physical and chemical

properties of a cellular lipid membrane. A second limitation is the use of the mini-G_s protein. Mini-G_s was designed to mimic the binding of full-length $G\alpha_S$ as a more robust, easily expressible variant, and thus regions of the native $G\alpha_S$ protein were removed, and point mutations were introduced, to create this engineered variant. Also, mini-G_s does not contain posttranslational modifications found in native $G\alpha_S$ such as palmitoylation, which anchors $G\alpha_S$ to the membrane surface in cells.

STAR★METHODS

Detailed methods are provided in the online version of this paper and include the following:

- KEY RESOURCES TABLE
- RESOURCE AVAILABILITY
  - Lead contact
  - Materials availability
  - Data and code availability
- EXPERIMENTAL MODEL AND SUBJECT DETAILS
- METHOD DETAILS
  - DNA constructs
  - $A_{2A}AR$ expression and purification
  - Mini-G_s expression and purification
  - Preparation and validation of $A_{2A}AR$–mini-G_s complexes
  - NMR experiments
- QUANTIFICATION AND STATISTICAL ANALYSIS

SUPPLEMENTAL INFORMATION

Supplemental information can be found online at https://doi.org/10.1016/j.celrep.2022.111844.

ACKNOWLEDGMENTS

We acknowledge National Institutes of Health grant numbers R35GM138291 (G.F. and M.T.E.) and R35GM138291-03S1 (M.T.E.). L.O.S. acknowledges funding from NIH training grant T32GM136583. A portion of this work was supported by the McKnight Brain Institute at the National High Magnetic Field Laboratory's AMRIS Facility, which is funded by National Science Foundation Cooperative agreement no. DMR-1644779 and the state of Florida.

AUTHOR CONTRIBUTIONS

G.F. and M.T.E. designed the experiments. G.F., K.A., L.O.S., N.T., and A.P.R. performed the biochemistry experiments. G.F. performed the NMR experiments and analyzed the data with M.T.E. All authors discussed the results and associated conclusions. G.F. and M.T.E. wrote the manuscript, and all authors approved the final version.

DECLARATION OF INTERESTS

The authors declare no competing interests.

Received: August 24, 2022
Revised: November 3, 2022
Accepted: November 24, 2022
Published: December 20, 2022

REFERENCES

1. Hauser, A.S., Attwood, M.M., Rask-Andersen, M., Schiöth, H.B., and Gloriam, D.E. (2017). Trends in GPCR drug discovery: new agents, targets and indications. Nat. Rev. Drug Discov. *16*, 829–842. https://doi.org/10.1038/nrd.2017.178.
2. Hilger, D., Masureel, M., and Kobilka, B.K. (2018). Structure and dynamics of GPCR signaling complexes. Nat. Struct. Mol. Biol. *25*, 4–12. https://doi.org/10.1038/s41594-017-0011-7.
3. Weis, W.I., and Kobilka, B.K. (2018). The molecular basis of G protein–coupled receptor activation. Annu. Rev. Biochem. *87*, 897–919. https://doi.org/10.1146/annurev-biochem-060614-033910.
4. Congreve, M., de Graaf, C., Swain, N.A., and Tate, C.G. (2020). Impact of GPCR structures on drug discovery. Cell *181*, 81–91. https://doi.org/10.1016/j.cell.2020.03.003.
5. Wacker, D., Stevens, R.C., and Roth, B.L. (2017). How ligands illuminate GPCR molecular pharmacology. Cell *170*, 414–427. https://doi.org/10.1016/j.cell.2017.07.009.
6. Shimada, I., Ueda, T., Kofuku, Y., Eddy, M.T., and Wüthrich, K. (2019). GPCR drug discovery: integrating solution NMR data with crystal and cryo-EM structures. Nat. Rev. Drug Discov. *18*, 59–82. https://doi.org/10.1038/nrd.2018.180.
7. Casiraghi, M., Banères, J.-L., and Catoire, L.J. (2017). NMR spectroscopy for the characterization of GPCR energy landscapes. In Structure and Function of GPCRs, G. Lebon, ed. (Springer International Publishing), pp. 27–52.
8. Nygaard, R., Zou, Y., Dror, R.O., Mildorf, T.J., Arlow, D.H., Manglik, A., Pan, A.C., Liu, C.W., Fung, J.J., Bokoch, M.P., et al. (2013). The dynamic process of β2-adrenergic receptor activation. Cell *152*, 532–542. https://doi.org/10.1016/j.cell.2013.01.008.
9. Ferré, G., and Eddy, M.T. (2020). Structural biology of human GPCR drugs and endogenous ligands - insights from NMR spectroscopy. Methods *180*, 79–88. https://doi.org/10.1016/j.ymeth.2020.08.008.
10. Ferré, G., Louet, M., Saurel, O., Delort, B., Czaplicki, G., M'Kadmi, C., Damian, M., Renault, P., Cantel, S., Gavara, L., et al. (2019). Structure and dynamics of G protein-coupled receptor–bound ghrelin reveal the critical role of the octanoyl chain. Proc. Natl. Acad. Sci. USA *116*, 17525–17530. https://doi.org/10.1073/pnas.1905105116.
11. Park, S.H., and Lee, J.H. (2020). Dynamic G protein-coupled receptor signaling probed by solution NMR spectroscopy. Biochemistry *59*, 1065–1080. https://doi.org/10.1021/acs.biochem.0c00032.
12. Ferré, G., Czaplicki, G., Demange, P., and Milon, A. (2019). Chapter Two - structure and dynamics of dynorphin peptide and its receptor. In Vitamins and Hormones, G. Litwack, ed. (Academic Press), pp. 17–47.
13. Frei, J.N., Broadhurst, R.W., Bostock, M.J., Solt, A., Jones, A.J.Y., Gabriel, F., Tandale, A., Shrestha, B., and Nietlispach, D. (2020). Conformational plasticity of ligand-bound and ternary GPCR complexes studied by 19F NMR of the β1-adrenergic receptor. Nat. Commun. *11*, 669. https://doi.org/10.1038/s41467-020-14526-3.
14. Manglik, A., Kim, T.H., Masureel, M., Altenbach, C., Yang, Z., Hilger, D., Lerch, M.T., Kobilka, T.S., Thian, F.S., Hubbell, W.L., et al. (2015). Structural insights into the dynamic process of β2-Adrenergic receptor signaling. Cell *161*, 1101–1111. https://doi.org/10.1016/j.cell.2015.04.043.
15. Ma, X., Hu, Y., Batebi, H., Heng, J., Xu, J., Liu, X., Niu, X., Li, H., Hildebrand, P.W., Jin, C., and Kobilka, B.K. (2020). Analysis of β2AR-Gs and β2AR-Gi complex formation by NMR spectroscopy. Proc. Natl. Acad. Sci. USA *117*, 23096–23105. https://doi.org/10.1073/pnas.2009786117.
16. Sounier, R., Mas, C., Steyaert, J., Laeremans, T., Manglik, A., Huang, W., Kobilka, B.K., Déméné, H., and Granier, S. (2015). Propagation of conformational changes during μ-opioid receptor activation. Nature *524*, 375–378. https://doi.org/10.1038/nature14680.

17. Grahl, A., Abiko, L.A., Isogai, S., Sharpe, T., and Grzesiek, S. (2020). A high-resolution description of β1-adrenergic receptor functional dynamics and allosteric coupling from backbone NMR. Nat. Commun. *11*, 2216. https://doi.org/10.1038/s41467-020-15864-y.

18. Isogai, S., Deupi, X., Opitz, C., Heydenreich, F.M., Tsai, C.-J., Brueckner, F., Schertler, G.F.X., Veprintsev, D.B., and Grzesiek, S. (2016). Backbone NMR reveals allosteric signal transduction networks in the β1-adrenergic receptor. Nature *530*, 237–241. https://doi.org/10.1038/nature16577.

19. Rößler, P., Mayer, D., Tsai, C.-J., Veprintsev, D.B., Schertler, G.F.X., and Gossert, A.D. (2020). GPCR activation states induced by nanobodies and mini-G proteins compared by NMR spectroscopy. Molecules *25*, 5984. https://doi.org/10.3390/molecules25245984.

20. Kull, B., Svenningsson, P., and Fredholm, B.B. (2000). Adenosine A_{2A} receptors are colocalized with and activate G_{olf} in rat striatum. Mol. Pharmacol. *58*, 771–777. https://doi.org/10.1124/mol.58.4.771.

21. Borea, P.A., Gessi, S., Merighi, S., Vincenzi, F., and Varani, K. (2018). Pharmacology of adenosine receptors: the state of the art. Physiol. Rev. *98*, 1591–1625. https://doi.org/10.1152/physrev.00049.2017.

22. Fredholm, B.B., Ijzerman, A.P., Jacobson, K.A., Klotz, K.-N., and Linden, J. (2001). International Union of Pharmacology. XXV. Nomenclature and classification of adenosine receptors. Pharmacol. Rev. *53*, 527–552.

23. Chen, J.-F., Eltzschig, H.K., and Fredholm, B.B. (2013). Adenosine receptors as drug targets — what are the challenges? Nat. Rev. Drug Discov. *12*, 265–286. https://doi.org/10.1038/nrd3955.

24. de Lera Ruiz, M., Lim, Y.-H., and Zheng, J. (2014). Adenosine A2A receptor as a drug discovery target. J. Med. Chem. *57*, 3623–3650. https://doi.org/10.1021/jm4011669.

25. Carpenter, B., and Lebon, G. (2017). Human adenosine A2A receptor: molecular mechanism of ligand binding and activation. Front. Pharmacol. *8*, 898. https://doi.org/10.3389/fphar.2017.00898.

26. Lebon, G., Warne, T., Edwards, P.C., Bennett, K., Langmead, C.J., Leslie, A.G.W., and Tate, C.G. (2011). Agonist-bound adenosine A2A receptor structures reveal common features of GPCR activation. Nature *474*, 521–525. https://doi.org/10.1038/nature10136.

27. Liu, W., Chun, E., Thompson, A.A., Chubukov, P., Xu, F., Katritch, V., Han, G.W., Roth, C.B., Heitman, L.H., Ijzerman, A.P., et al. (2012). Structural basis for allosteric regulation of GPCRs by sodium ions. Science *337*, 232–236. https://doi.org/10.1126/science.1219218.

28. Xu, F., Wu, H., Katritch, V., Han, G.W., Jacobson, K.A., Gao, Z.-G., Cherezov, V., and Stevens, R.C. (2011). Structure of an agonist-bound human A2A adenosine receptor. Science *332*, 322–327. https://doi.org/10.1126/science.1202793.

29. Jaakola, V.-P., Griffith, M.T., Hanson, M.A., Cherezov, V., Chien, E.Y.T., Lane, J.R., Ijzerman, A.P., and Stevens, R.C. (2008). The 2.6 angstrom crystal structure of a human A2A adenosine receptor bound to an antagonist. Science *322*, 1211–1217. https://doi.org/10.1126/science.1164772.

30. Carpenter, B., Nehmé, R., Warne, T., Leslie, A.G.W., and Tate, C.G. (2016). Structure of the adenosine A2A receptor bound to an engineered G protein. Nature *536*, 104–107. https://doi.org/10.1038/nature18966.

31. Clark, L.D., Dikiy, I., Chapman, K., Rödström, K.E., Aramini, J., LeVine, M.V., Khelashvili, G., Rasmussen, S.G., Gardner, K.H., and Rosenbaum, D.M. (2017). Ligand modulation of sidechain dynamics in a wild-type human GPCR. Elife *6*, e28505. https://doi.org/10.7554/eLife.28505.

32. Huang, S.K., Pandey, A., Tran, D.P., Villanueva, N.L., Kitao, A., Sunahara, R.K., Sljoka, A., and Prosser, R.S. (2021). Delineating the conformational landscape of the adenosine A2A receptor during G protein coupling. Cell *184*, 1884–1894.e14. https://doi.org/10.1016/j.cell.2021.02.041.

33. Ye, L., Van Eps, N., Zimmer, M., Ernst, O.P., and Prosser, R.S. (2016). Activation of the A2A adenosine G-protein-coupled receptor by conformational selection. Nature *533*, 265–268. https://doi.org/10.1038/nature17668.

34. Mizumura, T., Kondo, K., Kurita, M., Kofuku, Y., Natsume, M., Imai, S., Shiraishi, Y., Ueda, T., and Shimada, I. (2020). Activation of adenosine A2A receptor by lipids from docosahexaenoic acid revealed by NMR. Sci. Adv. *6*, eaay8544. https://doi.org/10.1126/sciadv.aay8544.

35. Eddy, M.T., Martin, B.T., and Wüthrich, K. (2021). A2A adenosine receptor partial agonism related to structural rearrangements in an activation microswitch. Structure *29*, 170–176.e3. https://doi.org/10.1016/j.str.2020.11.005.

36. Eddy, M.T., Lee, M.-Y., Gao, Z.-G., White, K.L., Didenko, T., Horst, R., Audet, M., Stanczak, P., McClary, K.M., Han, G.W., et al. (2018). Allosteric coupling of drug binding and intracellular signaling in the A2A adenosine receptor. Cell *172*, 68–80.e12. https://doi.org/10.1016/j.cell.2017.12.004.

37. Eddy, M.T., Gao, Z.-G., Mannes, P., Patel, N., Jacobson, K.A., Katritch, V., Stevens, R.C., and Wüthrich, K. (2018). Extrinsic tryptophans as NMR probes of allosteric coupling in membrane proteins: application to the A2A adenosine receptor. J. Am. Chem. Soc. *140*, 8228–8235. https://doi.org/10.1021/jacs.8b03805.

38. Carpenter, B., and Tate, C.G. (2016). Engineering a minimal G protein to facilitate crystallisation of G protein-coupled receptors in their active conformation. Protein Eng. Des. Sel. *29*, 583–594. https://doi.org/10.1093/protein/gzw049.

39. Pervushin, K., Riek, R., Wider, G., and Wüthrich, K. (1997). Attenuated T2 relaxation by mutual cancellation of dipole–dipole coupling and chemical shift anisotropy indicates an avenue to NMR structures of very large biological macromolecules in solution. Proc. Natl. Acad. Sci. USA *94*, 12366–12371.

40. Schwartz, T.W., Frimurer, T.M., Holst, B., Rosenkilde, M.M., and Elling, C.E. (2006). Molecular mechanism of 7TM receptor activation—a global toggle switch model. Annu. Rev. Pharmacol. Toxicol. *46*, 481–519. https://doi.org/10.1146/annurev.pharmtox.46.120604.141218.

41. Shi, L., Liapakis, G., Xu, R., Guarnieri, F., Ballesteros, J.A., and Javitch, J.A. (2002). β2 adrenergic receptor activation: modulation of the proline kink in transmembrane 6 by a rotamer toggle switch. J. Biol. Chem. *277*, 40989–40996. https://doi.org/10.1074/jbc.M206801200.

42. Ballesteros, J.A., and Weinstein, H. (1995). Integrated methods for the construction of three-dimensional models and computational probing of structure-function relations in G protein-coupled receptors. In Methods in Neurosciences (Elsevier), pp. 366–428.

43. Wacker, D., Wang, C., Katritch, V., Han, G.W., Huang, X.-P., Vardy, E., McCorvy, J.D., Jiang, Y., Chu, M., Siu, F.Y., et al. (2013). Structural features for functional selectivity at serotonin receptors. Science *340*, 615–619. https://doi.org/10.1126/science.1232808.

44. Sušac, L., Eddy, M.T., Didenko, T., Stevens, R.C., and Wüthrich, K. (2018). A2A adenosine receptor functional states characterized by 19F-NMR. Proc. Natl. Acad. Sci. USA *115*, 12733–12738. https://doi.org/10.1073/pnas.1813649115.

45. García-Nafría, J., Lee, Y., Bai, X., Carpenter, B., and Tate, C.G. (2018). Cryo-EM structure of the adenosine A2A receptor coupled to an engineered heterotrimeric G protein. Elife *7*, e35946. https://doi.org/10.7554/eLife.35946.

46. Dror, R.O., Arlow, D.H., Maragakis, P., Mildorf, T.J., Pan, A.C., Xu, H., Borhani, D.W., and Shaw, D.E. (2011). Activation mechanism of the β_2-adrenergic receptor. Proc. Natl. Acad. Sci. USA *108*, 18684–18689. https://doi.org/10.1073/pnas.1110499108.

47. Holst, B., Nygaard, R., Valentin-Hansen, L., Bach, A., Engelstoft, M.S., Petersen, P.S., Frimurer, T.M., and Schwartz, T.W. (2010). A conserved aromatic lock for the tryptophan rotameric switch in TM-VI of seven-transmembrane receptors. J. Biol. Chem. *285*, 3973–3985. https://doi.org/10.1074/jbc.M109.064725.

48. Yuan, S., Hu, Z., Filipek, S., and Vogel, H. (2014). W246 $^{6.48}$ opens a gate for a continuous intrinsic water pathway during activation of the adenosine A $_{2A}$ receptor. Angew. Chem. Int. Ed. Engl. *127*, 566–569. https://doi.org/10.1002/anie.201409679.

49. Lee, Y., Kim, S., Choi, S., and Hyeon, C. (2016). Ultraslow water-mediated transmembrane interactions regulate the activation of A 2A adenosine

receptor. Biophys. J. *111*, 1180–1191. https://doi.org/10.1016/j.bpj.2016.08.002.

50. Massink, A., Louvel, J., Adlere, I., van Veen, C., Huisman, B.J.H., Dijksteel, G.S., Guo, D., Lenselink, E.B., Buckley, B.J., Matthews, H., et al. (2016). 5′-Substituted amiloride derivatives as allosteric modulators binding in the sodium ion pocket of the adenosine A2A receptor. J. Med. Chem. *59*, 4769–4777. https://doi.org/10.1021/acs.jmedchem.6b00142.
51. Suzuki, S., Iida, M., Hiroaki, Y., Tanaka, K., Kawamoto, A., Kato, T., and Oshima, A. (2022). Structural insight into the activation mechanism of MrgD with heterotrimeric Gi-protein revealed by cryo-EM. Commun. Biol. *5*, 707. https://doi.org/10.1038/s42003-022-03668-3.
52. Wüthrich, K., and Wagner, G. (1975). NMR investigations of the dynamics of the aromatic amino acid residues in the basic pancreatic trypsin inhibitor. FEBS Lett. *50*, 265–268.
53. Wagner, G., DeMarco, A., and Wüthrich, K. (1976). Dynamics of the aromatic amino acid residues in the globular conformation of the basic pancreatic trypsin inhibitor (BPTI). Biophys. Struct. Mech. *2*, 159–180.
54. Mariño Pérez, L., Ielasi, F.S., Bessa, L.M., Maurin, D., Kragelj, J., Blackledge, M., Salvi, N., Bouvignies, G., Palencia, A., and Jensen, M.R. (2022). Visualizing protein breathing motions associated with aromatic ring flipping. Nature *602*, 695–700. https://doi.org/10.1038/s41586-022-04417-6.
55. Campbell, I.D., Dobson, C.M., and Williams, R.J. (1975). Proton magnetic resonance studies of the tyrosine residues of hen lysozyme-assignment and detection of conformational mobility. Proc. R. Soc. Lond. B Biol. Sci. *189*, 503–509.
56. Wei, S., Thakur, N., Ray, A.P., Jin, B., Obeng, S., McCurdy, C.R., McMahon, L.R., Gutiérrez-de-Terán, H., Eddy, M.T., and Lamichhane, R. (2022). Slow conformational dynamics of the human A2A adenosine receptor are temporally ordered. Structure *30*, 329–337.e5. https://doi.org/10.1016/j.str.2021.11.005.
57. Ali, R., Clark, L.D., Zahm, J.A., Lemoff, A., Ramesh, K., Rosenbaum, D.M., and Rosen, M.K. (2019). Improved strategy for isoleucine 1H/13C methyl labeling in Pichia pastoris. J. Biomol. NMR *73*, 687–697. https://doi.org/10.1007/s10858-019-00281-1.
58. Thakur, N., Wei, S., Ray, A.P., Lamichhane, R., and Eddy, M.T. (2022). Production of human A2AAR in lipid nanodiscs for 19F-NMR and single-molecule fluorescence spectroscopy. STAR Protoc. *3*, 101535. https://doi.org/10.1016/j.xpro.2022.101535.
59. Carpenter, B., and Tate, C.G. (2017). Expression and purification of mini G proteins from escherichia coli. Bio. Protoc. *7*, e2235. https://doi.org/10.21769/BioProtoc.2235.

STAR★METHODS

KEY RESOURCES TABLE

REAGENT or RESOURCE	SOURCE	IDENTIFIER
Antibodies		
Mouse monoclonal anti-FLAG M2 Alkaline Phosphatase	Sigma-Aldrich	Cat#A9469; RRID: AB_439699
Bacterial and virus strains		
E. coli BL21-CodonPlus (DE3)-RIL (chemocompetent)	Agilent	Cat#230245
Chemicals, peptides, and recombinant proteins		
PmeI	NEB	Cat#R0560L
Yeast nitrogen base (YNB) without amino acids and ammonium sulfate	Sigma-Aldrich	Cat#Y1251
^{15}N-labeled ammonium sulfate	CIL	Cat#NLM-713-50
Deuterium oxide ($^{2}H_2O$)	CIL	Cat#DLM-4-99.8
Theophylline	Sigma-Aldrich	Cat# T1633
Terrific Broth (TB)	RPI	Cat#T15000–1000.0
Biotin	Sigma-Aldrich	Cat#B4639
Iodoacetamide	Sigma-Aldrich	Cat#I1149
Lauryl maltose neopentyl glycol (LMNG)	Anatrace	Cat#NG310
Cholesteryl hemisuccinate (CHS)	Anatrace	Cat#CH210
Adenosine 5′-triphosphate (ATP)	Sigma-Aldrich	Cat#A2383
ZM241385: 4-(2-[7-Amino-2-(2-furyl)[1,2,4]triazolo[2,3-a][1,3,5]triazin-5-ylamino]ethyl)phenol	Tocris	Cat#1036
NECA: 5′-N-ethylcarboxamidoadenosine	Tocris	Cat#1691
Guanosine 5′-diphosphate (GDP)	Sigma-Aldrich	Cat#G7127
Apyrase	NEB	Cat#M0398S
Experimental models: Organisms/strains		
P. pastoris BG12 (electrocompetent)	BioGrammatics	Cat#PS004-01
Recombinant DNA		
pPIC9K-A_{2A}AR	Eddy et al., 2018[36]	N/A
pPIC9K-A_{2A}AR-W246$^{6.48}$F	Eddy et al., 2018[36]	N/A
pET15b-Mini-Gs	Carpenter et al., 2016[30]	N/A
Software and algorithms		
Topspin version 3.6.3	Bruker	https://www.bruker.com/en/products-and-solutions/mr/nmr-software.html
Other		
TALON resin	Clontech	Cat#635504
Ni-NTA resin	ThermoFisher	Cat# 88222
His-Trap HP NiNTA 5 mL column	Cytiva	Cat#17524802
PD-10	Cytiva	Cat#17085101
PD MiniTrap G25 column	Cytiva	Cat#28918007
HiPrep 26/10 column	Cytiva	Cat#17508701
HiLoad Superdex 75 column	Cytiva	Cat#90100805
Increase Superdex 200 10/300 GL column	Cytiva	Cat#28990944

RESOURCE AVAILABILITY

Lead contact

Further information and requests for resources and reagents should be directed to the lead contact, Matthew T. Eddy (matthew.eddy@chem.ufl.edu).

Materials availability

This study did not generate new or unique reagents.

Data and code availability

- All data reported in this paper will be shared by the lead contact upon request.
- This paper does not report original code.
- Any additional information required to reanalyze the data reported in this paper is available from the lead contact upon request.

EXPERIMENTAL MODEL AND SUBJECT DETAILS

XL10-Gold *E. coli* cells (Agilent) and *E. coli* BL21-CodonPlus (DE3)-RIL cells (Agilent) were cultivated in luria broth (LB) or terrific broth (TB) medium (RPI). The Bg12 strain of *P. pastoris* (Biogrammatics) was cultured in buffered minimal glycerol (BMGY) or buffered minimal methanol (BMMY) media containing yeast nitrogen base (Sigma-Aldrich). All cell lines used in this study were authenticated by the suppliers and were chosen to remain consistent with previous studies.

METHOD DETAILS

DNA constructs

We used published and pharmacologically validated constructs to produce A_{2A}AR and A_{2A}AR[W246F] in *P. pastoris.*[36,56] These constructs encode residues 1–316 of human A_{2A}AR by deletion of 96 C-terminal residues, an N154Q mutation to remove a putative glycosylation site, N-terminal FLAG tag and a C-terminal 10 X polyhistidine tag. Genes were cloned into the open reading frame of the pPIC9K expression vector at the BamHI and NotI sites, eliminating the α-factor secretion signal present in the original vector.

We used a construct to produce mini-G_s described in the literature,[30] which was cloned into the pET15b expression vector.

A_{2A}AR expression and purification

We expressed and purified A_{2A}AR and A_{2A}AR[W246F] following established procedures,[36,57,58] described in detail below. Expression plasmids were linearized using PmeI and transformed by electroporation into *P. pastoris* BG12 cells. Clones were then screened in 4 mL cultures for receptor expression using an anti-FLAG Western blot analysis.[58]

For expression of unlabeled A_{2A}AR and A_{2A}AR[W246F], selected clones were grown for 2 days at 30°C in 4 mL of BMGY medium (4.25 g/L YNB without amino acids and ammonium sulfate, 11.7 g/L NaH_2PO_4, 7.5 g/L Na_2HPO_4, 5 g/L ammonium sulfate, 20 g/L glycerol, 2 μM biotin) with 100 μg/mL carbenicillin. Starter cultures were used to inoculate 50 mL of the same medium, grown for 3 days at 30°C, then used to inoculate 500 mL cultures in enriched BMGY medium (8.5 g/L YNB without amino acids and ammonium sulfate, 11.7 g/L NaH_2PO_4, 7.5 g/L Na_2HPO_4, 10 g/L ammonium sulfate, 20 g/L glycerol, 2 μM biotin) with 100 μg/mL carbenicillin. These large scale cultures were grown for 2 days at 30°C then at 28°C for 8 h 1 mM theophylline was added to the cultures, and A_{2A}AR or A_{2A}AR[W246F] expression was induced over 40 h at 28°C by addition of 5 g/L methanol every ~13 h (15 g/L total). Cells were sedimented at 3000 x g and 4°C for 15 min and frozen at −80°C until needed. Thawed cells were suspended in ice-cold 50 mM sodium phosphate pH 7.0, 100 mM NaCl, 5% w/v glycerol with 1 X in-house EDTA-free protease inhibitor cocktail (500 μM AEBSF, 1 μM E−64, 1 μM leupeptin, 150 nM aprotinin) and lysed with a cell disruptor operating at 40 kPsi and 7°C. Membrane fractions containing A_{2A}AR were sedimented by ultracentrifugation at 220,000 x g and 4°C for 30 min and stored at −80°C until further use.

The following modifications to the above procedure were used for expression of [u-^{15}N,~70% ^{2}H]-A_{2A}AR and [u-^{15}N,~70% ^{2}H]-A_{2A}AR[W246F]. Cells were progressively adapted to $^{2}H_2O$ by growing them at 30°C in 4 mL of BMGY medium (4.25 g/L YNB without amino acids and ammonium sulfate, 11.7 g/L NaH_2PO_4, 7.5 g/L Na_2HPO_4, 5 g/L unlabeled ammonium sulfate, 20 g/L glycerol, 2 μM biotin) with 100 μg/mL carbenicillin and increasing concentrations of $^{2}H_2O$. These cultures were twice inoculated in media prepared with 90% v/v $^{2}H_2O$ and allowed to grow for 3–5 days, then inoculated in media prepared with 99.5% v/v $^{2}H_2O$, allowed to grow for 7 days, and scaled up to 50 mL and 500 mL cultures in labeled BMGY (4.25 g/L YNB without amino acids and ammonium sulfate, 11.7 g/L NaH_2PO_4, 7.5 g/L Na_2HPO_4, 5 g/L ^{15}N-labeled ammonium sulfate, 20 g/L glycerol, 2 μM biotin, 99.5% v/v $^{2}H_2O$) with 100 μg/mL carbenicillin. Before lowering the incubation temperature to 28°C, cells were centrifuged at 3000 x g and 4°C for 30 min and exchanged into labeled BMMY medium (4.25 g/L YNB without amino acids and ammonium sulfate, 11.7 g/L NaH_2PO_4, 7.5 g/L Na_2HPO_4, 5 g/L ^{15}N-labeled ammonium sulfate, 2 μM biotin, 99.5% v/v $^{2}H_2O$) with 100 μg/mL carbenicillin. Protein expression, cells lysis and membrane fraction collection were performed in the same manner as for unlabeled A_{2A}AR.

All A_{2A}AR and A_{2A}AR[W246F] samples were purified with the same procedure. Every step was performed at 4°C or on ice. Thawed membranes were resuspended in buffer containing 10 mM HEPES pH 7.0, 1 M NaCl, 10 mM KCl, 20 mM $MgCl_2$ followed by ultracentrifugation at 220,000 x g and 4°C for 30 min. The pellet was then resuspended in the same buffer containing 2 mg/mL iodoacetamide, 1 mg/mL theophylline and 1 X protease inhibitor cocktail (see composition above) for 1 h. Resuspended membranes were mixed with the same volume of 2 X solubilization buffer (10 mM HEPES pH 7.0, 500 mM NaCl, 0.5% w/v LMNG, 0.025% w/v CHS) and incubated for 4.5 h at 4°C. Solubilized material was clarified by ultracentrifugation at 220,000 x g and 4°C for 30 min and the supernatant incubated overnight with TALON resin and 30 mM imidazole. TALON-bound A_{2A}AR or A_{2A}AR[W246F] was washed by

successive steps of resuspension in buffers and sedimentation at 850 x g for 15 min, first with buffer containing 25 mM HEPES pH 7.0, 500 mM NaCl, 10 mM $MgCl_2$, 30 mM imidazole, 8 mM ATP, 0.1% w/v LMNG, 0.005% w/v CHS, then twice with buffer containing 25 mM HEPES pH 7.0, 250 mM NaCl, 30 mM imidazole, 5% glycerol, 0.05% w/v LMNG, 0.0025% w/v CHS, and 100 μM ligand (NECA or ZM241385). A_{2A}AR or A_{2A}AR[W246F] was eluted from the resin in gravity flow columns with buffer containing 25 mM HEPES pH 7.0, 250 mM NaCl, 300 mM imidazole, 5% glycerol, 0.05% w/v LMNG, 0.0025% w/v CHS, 100 μM ligand. Eluted A_{2A}AR or A_{2A}AR[W246F] was exchanged into the final buffer with PD-10 columns equilibrated with 25 mM HEPES pH 7.0, 75 mM NaCl, 5 mM $MgCl_2$, 0.03% w/v LMNG, 0.0015% w/v CHS, 100 μM ligand (NECA or ZM241385). The purity and monodispersity of A_{2A}AR or A_{2A}AR[W246F] in LMNG/CHS was validated by analytical SEC using a Sepax Nanofilm SEC-250 column equilibrated with 25 mM HEPES pH 7.0, 75 mM NaCl, 5 mM $MgCl_2$, 0.03% w/v LMNG, 0.0015% w/v CHS (Figure S1A).

Mini-G_s expression and purification

We produced mini-G_s using a strategy adapted from the literature,[38,59] described in more detail as follows. *E. coli* BL21-CodonPlus (DE3)-RIL cells were transformed with the expression vector and cultivated at 30°C in TB medium with 0.2% glucose, 34 μg/mL chloramphenicol, 100 μg/mL carbenicillin and 5 mM $MgSO_4$. Protein expression was induced with 50 μM IPTG, and cells were grown at 25°C for an additional 20 h after induction. The cells were then sedimented at 3000 x g and 4°C for 15 min and stored at −80°C. Every purification step was performed at 4°C or on ice. Lysis was performed in ice-cold 40 mM HEPES pH 7.5, 100 mM NaCl, 10 mM imidazole, 10% v/v glycerol, 5 mM $MgCl_2$, 50 μM GDP with 1 X protease inhibitor cocktail (see composition above) using a cell disruptor at operating 20 kPsi and 7°C. The lysate was clarified by centrifugation at 75,000 x g and 10°C for 30 min and loaded on a His-Trap HP NiNTA 5 mL column for IMAC purification. The resin was washed and the protein was eluted with buffer containing 40 mM and 400 mM imidazole, respectively. Eluted protein was exchanged into buffer using a HiPrep 26/10 column equilibrated with 20 mM HEPES pH 7.5, 100 mM NaCl, 10% v/v glycerol, 1 mM $MgCl_2$, and 10 μM GDP. Mini-G_s was incubated overnight with SuperTEV protease at 1/100 molar ratio. SuperTEV and undigested mini-G_s were removed by reverse IMAC by incubating the sample mixture with Ni-NTA resin and 30 mM imidazole for 1 h and collecting the flow through containing mini-G_s. The digested mini-G_s was further purified by SEC using a HiLoad Superdex 75 column equilibrated in 10 mM HEPES pH 7.5, 100 mM NaCl, 10% v/v glycerol, 1 mM $MgCl_2$, 1 μM GDP, 0.1 mM TCEP. The samples were frozen in liquid nitrogen and stored at −80°C before buffer exchange with a PD-10 desalting column equilibrated with 25 mM HEPES pH 7.0, 75 mM NaCl, 5 mM $MgCl_2$, 100 μM TCEP, 1 μM GDP.

Preparation and validation of A_{2A}AR−mini-G_s complexes

A_{2A}AR was concentrated to ∼300 μM and mini-G_s was concentrated to ∼3.3 mM. The two separate solutions were then mixed together and 0.1 U apyrase was added to prepare samples with ∼250 μM A_{2A}AR and 1.2 to 1.8 molar equivalent of mini-G_s in buffer containing 25 mM HEPES pH 7.0, 75 mM NaCl, 5 mM $MgCl_2$, 0.027% w/v LMNG, 0.00135% w/v CHS, 90 μM ligand, ≤10 μM TCEP, ≤0.1 μM GDP. Complexes of A_{2A}AR[W246F] and mini-G_s were prepared by first mixing the two proteins then concentrating to obtain samples with ∼150 μM receptor and 1.5 to 1.9 molar equivalent of mini-G_s as this procedure proved to be more robust. All samples were then incubated overnight at 4°C prior to starting experiments the following morning.

To assess complex formation of A_{2A}AR−mini-G_s and A_{2A}AR[W246F]−mini-G_s, samples were analyzed by SEC (Figures 1, S1B, and S1C) using a Superdex Increase 200 10/300 GL column equilibrated at 4°C in 25 mM HEPES pH 7.0, 75 mM NaCl, 5 mM $MgCl_2$, 0.025% w/v LMNG, 0.00125% w/v CHS. The amount of A_{2A}AR−mini-G_s complex formed was evaluated from the quantity of free mini-G_s and consideration of the stoichiometry of A_{2A}AR and mini-G_s, as compared to reference samples with the mini-G_s alone. Fractions containing A_{2A}AR−mini-G_s complexes were collected and the presence of both mini-G_s and A_{2A}AR contained within the same fraction was confirmed by SDS-PAGE. SDS-PAGE samples were prepared with 50 mM DTT and analyzed using 12% acrylamide Tris-Tricine gels stained with Coomassie blue.

NMR experiments

[u-^{15}N,∼70% ^{2}H]-A_{2A}AR and [u-^{15}N,∼70% ^{2}H]-A_{2A}AR[W246F] samples were prepared according to the above procedure then exchanged into NMR buffer with a PD MiniTrap G25 column equilibrated with 25 mM HEPES pH 7.0, 75 mM NaCl, 5 mM $MgCl_2$, 0.025% w/v LMNG, 0.00125% w/v CHS, and excess ligand. Samples were concentrated and supplemented with 10% v/v $^{2}H_2O$ to final concentrations of 260 μM for A_{2A}AR (with 310 μM mini-G_s) and 140 μM for A_{2A}AR[W246F] (with 260 μM mini-G_s).

After recording NMR experiments with A_{2A}AR in complex with NECA and mini-G_s, the complexes were dissociated by ligand exchange. The sample was 7-fold diluted in NMR buffer containing 100 μM ZM241385 and incubated at 4°C for 6 h. Excess free NECA was removed by exchanging the sample buffer using a PD-10 column equilibrated with NMR buffer containing 100 μM ZM241385. The sample was then concentrated to 200 μM, supplemented with 10% v/v $^{2}H_2O$ to record NMR data.

All samples were pipetted into 5 mm Shigemi tubes, and NMR data were recorded at 34°C and 800 MHz with a Bruker Avance III spectrometer equipped with a 5 mm TXI cryoprobe. Data were acquired with Topspin version 3.6.3 and analyzed with NMRFAM-Sparky 1.470. 2D [^{15}N,^{1}H]-TROSY spectra were recorded with 2048 and 256 points in the direct and indirect dimensions, respectively. TROSY spectra of [u-^{15}N,∼70% ^{2}H]-A_{2A}AR in complexes with NECA or NECA and mini-G_S were recorded with 672 scans (∼54 h) and in complex with ZM241385 with 336 scans (∼27 h). The TROSY spectrum of [u-^{15}N,∼70% ^{2}H]-A_{2A}AR[W246F] in complex with NECA and mini-G_s was recorded with 832 scans (∼66 h). All spectra were processed identically: prior to Fourier transformation,

the data matrices were zero filled to 2048 (t1) x 4096 (t2) complex points and multiplied by a Gaussian window function (8.0 Hz LB and 0.1 GB) in the direct dimension and squared cosine window function in the indirect dimension.

QUANTIFICATION AND STATISTICAL ANALYSIS

The indole $^{15}N-^{1}H$ signals for W29, W32, W143, and W268 and backbone amide $^{15}N-^{1}H$ signals for G114, G118, G142, G158, G160 and G218 could be assigned for the complexes with mini-G_s from literature data recorded without mini-G_s.[35,36] The indole $^{15}N-^{1}H$ signal for W246 was assigned for complexes with mini-G_s using literature data and additional experiments with [u-^{15}N,~70% ^{2}H]-A_{2A}AR[W246F] in complex with NECA and mini-G_s (Figure S3). To rule out the possibility of unique indole $^{15}N-^{1}H$ signals for W246 in spectra of the A_{2A}AR complex with mini-G_s, we compared spectra of [u-^{15}N,~70% ^{2}H]-A_{2A}AR[W246F] in complex with NECA and mini-G_S and spectra of [u-^{15}N,~70% ^{2}H]-A_{2A}AR in complex with NECA and mini-G_s with additional spectra of [u-^{15}N,~70% ^{2}H]-A_{2A}AR in complex with ZM241385 or NECA. From this comparison, we concluded no new signals were observed in the tryptophan region and surrounding regions in the TROSY spectrum of the ternary complex with NECA and mini-G_S.

Chemical shift perturbations (CSP) reported in Figures 4A and 4B were calculated with the following equation:

$$CSP = \sqrt{(\omega_1 - \omega_2)_H^2 + (\omega_1 - \omega_2)_N^2}$$

where ω_1 and ω_2 are the resonance frequencies in Hertz of a given NMR signal for the compared spectra and *H* and *N* indicate the ^{1}H and ^{15}N dimensions, respectively. The intensity ratios, "I. ratio", reported in Figure 4A and B were calculated from the intensities at the signal maxima and normalized relative to the intensity of the indole $^{15}N-^{1}H$ signal for W268. This signal appeared to be unresponsive to changes in efficacy of bound ligands or the presence of mini-G_S, likely because of its placement in a flexible extracellular region, and thus was used as an internal control.